Distributed forcing of the flow past a blunt-based axisymmetric bluff body

Thierry Jardin · Yannick Bury

Abstract In this paper we address the influence of a blowing/suction-type distributed forcing on the flow past a blunt-based axisymmetric bluff body by means of direct numerical simulations. The forcing is applied *via* consecutive blowing and suction slots azimuthally distributed along the trailing edge of the bluff body. We examine the impact of the forcing wavelength, amplitude and waveform on the drag experienced by the bluff body and on the occurrence of the reflectional symmetry preserving (RSP) and reflectional symmetry breaking (RSB) wake modes, for Reynolds numbers 800 and 1000. We show that forcing the flow at wavelengths inherent to the unforced flow drastically damps drag oscillations associated with the vortex shedding and vorticity bursts, up to their complete suppression. The overall parameter analysis suggests that this damping results from the surplus of streamwise vorticity provided by the forcing, that tends to stabilize the ternary vorticity lobes observed at the aft part of the bluff body. In addition, conversely to a blowing-type or suction-type forcing, the blowing/suction-type forcing involves strong nonlinear interactions between locally decelerated and accelerated regions, severely affecting both the mean drag and the frequencies representative of the vortex shedding and vorticity bursts.

1 Introduction

Recent studies have demonstrated that massively separated flows past bluff bodies can be highly receptive to the excitation of specific flow instabilities. As such, instability-based flow control strategies can lead to drastic modifi-

T. Jardin · Y. Bury (✉)
Université de Toulouse, ISAE, Toulouse, 31055, France
E-mail: yannick.bury@isae.fr
Tel.: +33-561339198
Fax: +33-561339163

cations of the flow topology [6, 7], subsequently reducing aerodynamic loads, mitigating airframe noise or enhancing gas mixing.

In their contribution to the Annual Review of Fluid Mechanics [4], Choi and coworkers provide a comprehensive overview of flow control strategies on bluff bodies and highlight how effective 3D forcing can be for the reduction of drag of a 2D bluff body, when the forcing wavelength coincides with the wavelength of the most receptive flow instability. The forcing wavelength can be imposed through the geometrical modification of the bluff body along its spanwise direction (passive control) or through the spatial distribution of steady or pulsed jets (active control). The latter is referred to as distributed forcing.

[9] and [10] have emphasized the sensitivity of the flow past a circular cylinder to a continuously distributed steady forcing at wavelength close to mode A wake instability. They observed a drastic reduction of the drag experienced by the cylinder associated with the suppression of the von Kármán vortex shedding. Similarly [8] have obtained conclusive outcomes for the drag reduction of a 2D model vehicle.

According to these authors, the main reason for the distributed forcing efficiency observed on 2D bluff bodies relies on the dislocation of nominally 2D vortices into 3D structures. Since such efficiency appears to be closely linked to the resulting tri-dimensionalization of the bluff body wake, an important question arises: can distributed forcing still act as an efficient flow control strategy for 3D bluff bodies?

In an attempt to answer this question, we numerically investigate the influence of distributed forcing on the flow past a blunt-based axisymmetric bluff body. Indeed blunt-based axisymmetric bluff bodies exhibit complex three-dimensional wake topology, driven by various instabilities that can be considered as relevant targets for the definition of instability-based flow control strategies. These instabilities are associated with the occurrence of successive wake modes as the Reynolds number is increased, namely the SS, RSP and RSB wake states [1–3]. The SS state is known to be characterized by a 'double threaded' wake composed of two counter-rotating streamwise vortical structures. The wake is steady and exhibits a streamwise planar symmetry whose azimuthal position fixes randomly. As the Reynolds number is increased, the 'double threaded' wake evolves into unsteady hairpin structures, giving rise to the RSP state. The latter may be characterized by periodic and aperiodic vortex shedding that still preserve the wake planar symmetry. At even higher Reynolds numbers, the planar symmetry is broken, leading to the RSB state, and the wake exhibits a helical pattern due to the twisting of the hairpin structures. The present study focuses on a length-to-diameter ratio $L/D = 7$ axisymmetric bluff body for Reynolds numbers 800 and 1000, spanning the unsteady wake regimes RSP and RSB. A blowing/suction-type forcing is applied at the bluff body trailing edge and the influence of the forcing amplitude, wavelength and waveform is analysed.

2 Numerical methods

The three-dimensional time-dependent incompressible Navier-Stokes equations around a blunt-based axisymmetric bluff body are directly solved using a finite volume method. The bluff body is similar to that used in [3,11,12]. It consists in a 1:4 semi-elliptic nose and a cylindrical aft section of diameter D. The Reynolds number, based on D and on the free stream velocity U_∞ ranges from 800 to 1000. In the cartesian reference frame (O, x, y, z) the equations read:

$$\boldsymbol{\nabla}.\mathbf{v} = 0 \tag{1}$$

$$\frac{\partial \mathbf{v}}{\partial t} + (\mathbf{v}.\boldsymbol{\nabla})\mathbf{v} = -\frac{1}{\rho}\boldsymbol{\nabla} p + \nu \nabla^2 \mathbf{v} \tag{2}$$

Here $\mathbf{v}$ is the velocity, p the pressure, ρ and ν the fluid density and kinematic viscosity respectively.

The bluff body is enclosed in a cylindrical computational domain of diameter $20D$ and length $55D$ aligned with the free stream direction $\mathbf{x}$ (figure 1). The coordinates' origin O is located at the nose tip of the body, corresponding to the stagnation point. The inlet boundary is located at $x/D = -8$ and is subjected to a velocity Dirichlet condition. A similar condition is imposed on the tubular surface of the computational domain. A zero diffusion flux condition is prescribed at the outlet boundary located at $x/D = 47$. The surface of the blunt-based axisymmetric bluff body is modelled as non-slip surface. The blowing and suction forcing is applied at the bluff body trailing edge, normally to the body surface, through a $0.085D$ wide circumferential belt (figure 2). The latter is subjected to the following velocity Dirichlet condition:

$$U_r = \alpha U_\infty \times \xi(2\pi\theta/\lambda_\theta) \tag{3}$$

where α and λ_θ are the forcing amplitude and azimuthal wavelength respectively. θ refers to the azimuthal position in cylindrical coordinates (O, r, θ, x). $\xi()$ is a mathematical function that either stands for sin() or sgn(sin()), generating sine or square-type waveforms. In addition, the blowing or suction phases of the sine waveform can be turned off (an illustration of the waveforms is given in §3.2, figure 9). For each forcing case, forcing is applied once the unforced flow is fully established, at time unit $t^+ = tU_\infty/D = 175$.

The domain is composed of 2×10^6 hexahedral cells. The spatial and temporal discretizations are achieved using second-order upwind schemes and second-order implicit time-stepping method respectively. A semi-implicit iterative algorithm is employed for the pressure-velocity coupling. The time step is fixed in order to satisfy the CFL condition (maximum Courant Number below unity). A 175 time unit simulation results in a typical computation time in the order of 188 hours on a HP xw4600 workstation equipped with two Intel Core 2 Duo processors running at 2.93GHz. Note that halving the computation time step increases the computation time by 70%.

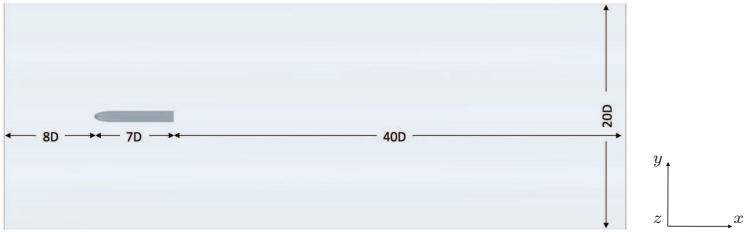

Fig. 1 Computational domain.

Fig. 2 Location of the distributed forcing (dark) on the trailing edge of the bluff body and illustration in the (y, z) plane of the azimuthal sine-type waveform at wavelength $\lambda_\theta = 2\pi/1$, $2\pi/2$, $2\pi/3$, $2\pi/4$ and $2\pi/5$, from left to right (blue circle depicts the trailing edge section. $+$ and $-$ symbols indicate regions of blowing and suction respectively).

Further simulations were carried out to ensure that the results are independent of the number of cells, the time step and the relative position of the boundary conditions. In particular, tests on the position of the tubular and outlet surfaces of the computational domain ensured that any reflecting-boundary issues disrupt instability occurrence. Besides, simulations using comparable settings have already shown the ability to accurately predict wake transitions past axisymmetric bluff bodies [1,3,13].

3 Results

In this section we investigate the influence of the forcing wavelength λ_θ, amplitude α and waveform ξ on the drag coefficient C_D experienced by the axisymmetric bluff body. To this avail we take advantage of the mechanistic analysis of the unforced case proposed in [3].

At $Re = 800$, the wake of the axisymmetric bluff body exhibits streamwise vortical structures, referred to as the primary lobes, periodically shed at a normalized frequency $St_a = f_a D/U_\infty \approx 0.12$ (figure 3(a)). The latter are distributed on both sides of a randomly fixed plane of symmetry (also visible on figure 6), typical of the RSP state. The vortex shedding is modulated by the occurrence of a secondary instability at $St_b = f_b D/U_\infty \approx 0.02$ responsible for the periodic discharge of the ternary lobes and the concomitant vorticity bursts observed on figure 3(b). While the impact of the vortex shedding on the bluff body drag fluctuations is barely visible on the time history of the drag coefficient whose mean value $\bar{C_D} \approx 0.675$, vorticity bursts induce significant C_D amplitude oscillations, of the order of $\Delta C_D \approx 0.02$, at normalized frequency St_b (plain line on figure 5). In addition, [3] brought to the fore the inception of chaos, characterized by intermittent restabilizations of the wake

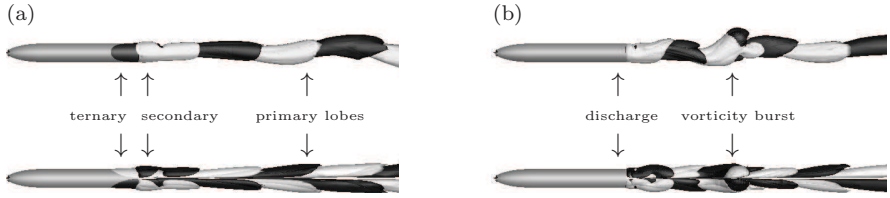

Fig. 3 Iso-surfaces of normalized streamwise vorticity $\omega^+ = \omega D/U_\infty = \pm 0.04$ (dark: positive, light: negative; upper line: side view, lower line: upper view) illustrating (a) vortex shedding and (b) vorticity bursts at $Re = 800$.

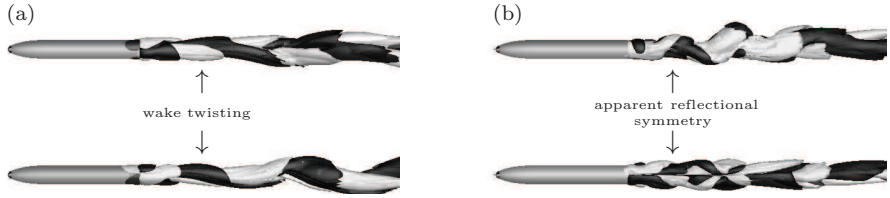

Fig. 4 Iso-surfaces of normalized streamwise vorticity $\omega^+ = \omega D/U_\infty = \pm 0.03$ (dark: positive, light: negative; upper line: side view, lower line: upper view) illustrating (a) wake twisting and (b) 'apparent' reflectional symmetry at $Re = 1000$.

and concomitant drag damping. Nonetheless the latter observations require very long-term computations and will thus not be addressed here.

At $Re = 1000$, the planar symmetry is broken. The onset of the helical mode intermittently promotes the wake twisting representative of the RSB state. The wake topology then consists in a succession of phases of 'apparent' reflectional symmetry, wake twisting and dramatic reorientation of the 'apparent' reflectional symmetry (figure 4). In addition, vortex shedding, vorticity bursts and intermittent restabilizations still persist beyond the bifurcation to the RSB state. The aperiodic reorganizations of the wake occur in conjunction with the intensification of the erratic fluctuations of the drag experienced by the bluff body, that superimpose with the periodic oscillations resulting from the vortex shedding and vorticity bursts, around the mean value $\bar{C_D} \approx 0.604$.

3.1 Influence of the forcing wavelength

3.1.1 $Re = 800$

Figure 5(a) displays the time history of the drag coefficient C_D for five distinct wavelengths λ_θ ranging from $2\pi/1$ to $2\pi/5$ at $Re = 800$. Here the forcing amplitude α is fixed to 0.1 and the forcing waveform ξ is a sine function. For the most representative forcing cases, normalized streamwise vorticity ω^+ contours at cross-sections located at the base and $1D$ downstream of the bluff body are illustrated on figure 6.

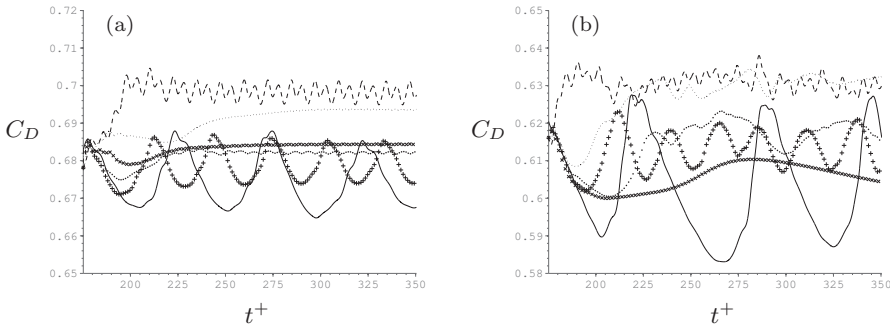

Fig. 5 Time history of the drag coefficient C_D as a function of the forcing wavelength λ_θ at $Re = 800$ (a) and $Re = 1000$ (b). — unforced; – – $\lambda_\theta = 2\pi/1$; $\cdots$ $\lambda_\theta = 2\pi/2$; $\times$ $\lambda_\theta = 2\pi/3$; $\cdots$ $\lambda_\theta = 2\pi/4$; $+$ $\lambda_\theta = 2\pi/5$.

At $\lambda_\theta = 2\pi/1$ the forcing is characterized by a plane of symmetry, directed along (x, y), on which the wake plane of symmetry ends up coinciding. Figure 6 shows that the vorticity lobes are symmetrically distributed on both sides of the (x, y) plane. Their associated vorticity levels are significantly enhanced in comparison with those observed for the unforced case, due to the sine-type waveform of the forcing that locally adds streamwise vorticity in the aft portion of the bluff body (illustrated on figure 9). Interestingly, this tends to fix the ternary lobes and mitigate their discharge in the wake. A striking consequence is the annihilation of the large amplitude/low frequency ($St_b \approx 0.02$) oscillations of the drag coefficient experienced by the bluff body (figure 5(a)). The latter, whose mean value noticeably increases compared to the unforced case, up to $\bar{C_D} \approx 0.698$, is now driven by the primary instability associated with the vortex shedding. Yet the shedding frequency St_a is shifted to $St_a \approx 0.16$ and modulated at a normalized frequency $St_a/2$. This subharmonics reveals the periodic variation of intensity between two successive counter-rotating primary lobes, present in the unforced case [1,3] but further amplified by the assymetry of the $\lambda_\theta = 2\pi/1$ sine-type forcing relatively to the (x, z) plane.

The $\lambda_\theta = 2\pi/2$ sine-type forcing has an even more dramatic effect on the drag experienced by the bluff body, as revealed by the complete inhibition of drag oscillations observed on figure 5. The mean drag coefficient slightly decreases compared to the previous case and fixes to $\bar{C_D} \approx 0.694$. Concomitantly one can observe the destructuration of the wake primary lobes, in the sense of the loss of planar symmetry, clearly visible on ω^+ cross-section located $1D$ downstream of the bluff body base (lower line of figure 6).

While a similar trend is noticed on the damping of the drag oscillations at $\lambda_\theta = 2\pi/3$, the wake recovers a planar symmetry whose orientation fixes on one of the forcing planes of symmetry. Therefore, and conversely to what has been observed for the distributed forcing of nominally 2D wakes [9], one might not expect a direct causal connection between the wake destructuration

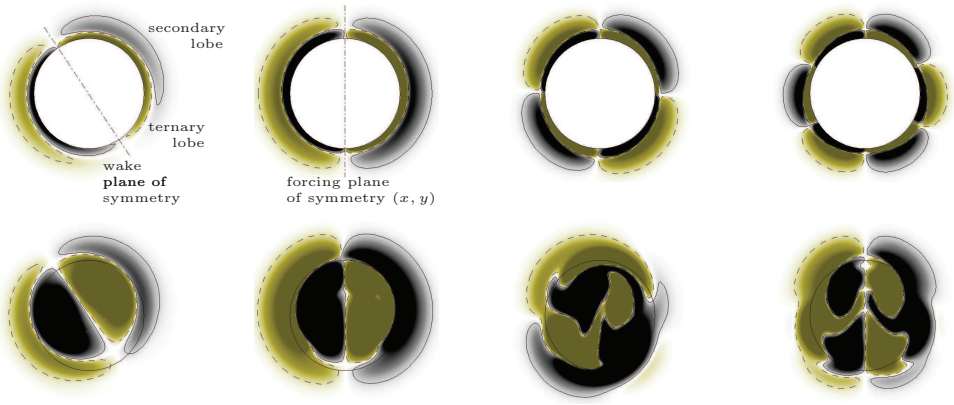

Fig. 6 Iso-contours and iso-lines of normalized streamwise vorticity (plain line: $\omega^+ = 0.02$, dashed line: $\omega^+ = -0.02$) at the base (upper line) and $1D$ downstream (lower line) of the bluff body, at $Re = 800$.

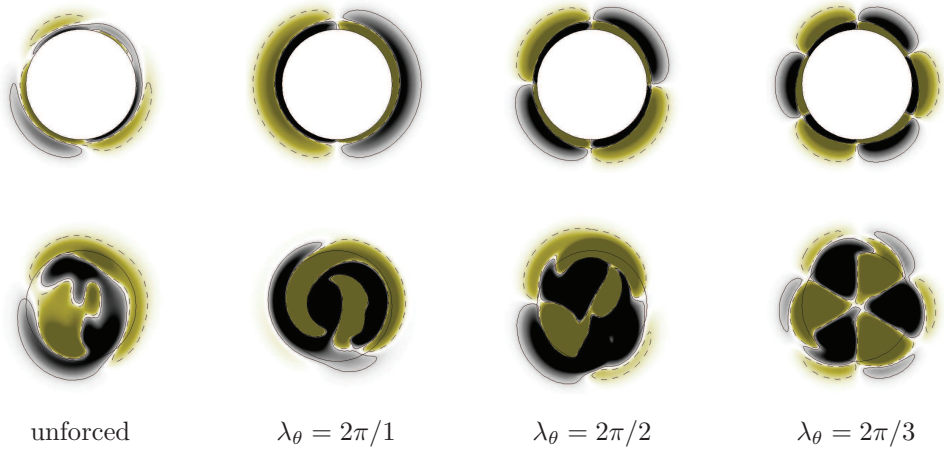

Fig. 7 Iso-contours and iso-lines of normalized streamwise vorticity (plain line: $\omega^+ = 0.01$, dashed line: $\omega^+ = -0.01$) at the base (upper line) and $1D$ downstream (lower line) of the bluff body, at $Re = 1000$.

and the annihilation of the drag oscillations in the case of an axisymmetric 3D bluff body.

At this stage, the further decrease of the forcing wavelength tends to restore the main characteristics of the unforced wake. As such, the mean drag coefficient $\bar{C_D}$ is reduced from 0.684 for $\lambda_\theta = 2\pi/3$ to 0.682 for $\lambda_\theta = 2\pi/4$ and 0.679 for $\lambda_\theta = 2\pi/5$. In parallel, drag oscillations associated with vortex shedding and vorticity bursts manifest anew at $\lambda_\theta = 2\pi/4$ with $St_a \approx 0.14$

and $\lambda_\theta = 2\pi/5$ with $St_b \approx 0.03$ respectively, while still preserving the wake planar symmetry (not shown here for sake of conciseness). Those Strouhal numbers differ from those reported for the unforced flow, due to the successive blowing and suction regions that locally affect the separation of the flow. The upstream flow tends to accelerate when approaching a suction region while it decelerates and experiences earlier separation when approaching a blowing region. As a consequence the global shedding process is affected by nonlinear interactions between locally accelerated or decelerated flow regions.

3.1.2 $Re = 1000$

Figure 5(b) depicts the influence of the forcing wavelength on the drag coefficient C_D at $Re = 1000$. Although the modal signature of the unforced wake differs from that at $Re = 800$, through the onset of the helical mode and the amplification of the chaotic state, the impact of the forcing on the temporal evolution of C_D at $Re = 1000$ exhibits strong similarities with that obtained at $Re = 800$. As such 1) the forcing at $\lambda_\theta = 2\pi/1$ still annihilates the large amplitude/low frequency oscillations of the drag coefficient, associated with the vorticity bursts; 2) the forcing at $\lambda_\theta = 2\pi/2$ and $\lambda_\theta = 2\pi/3$ damps the remaining drag coefficient oscillations associated with the vortex shedding; 3) the further decrease of the forcing wavelength down to $\lambda_\theta = 2\pi/5$ tends to restore the drag oscillations resulting from the vortex shedding and vorticity bursts. Here again the Strouhal number associated with the vorticity bursts is shifted (*e.g.* $St_b \approx 0.05$ for $\lambda_\theta = 2\pi/5$ while $St_b \approx 0.02$ for the unforced flow), still denoting the impact of interacting blowing and suction regions on the global shedding process.

Besides the progressive mitigation of the periodic oscillations of the drag coefficient experienced by the bluff body, when decreasing the wavelength from $\lambda_\theta = 2\pi/1$ to $\lambda_\theta = 2\pi/4$, spotlights the erratic drag fluctuations intrinsic to the chaotic unforced flow at $Re = 1000$. Note that the forcing at $Re = 800$ fully suppresses these erratic fluctuations, underlying the weakness of nascent chaos at this flow regime, *i.e.* slightly above $Re = 790$ [3]. At this point it is worth touching on the $\lambda_\theta = 2\pi/3$ forcing case. Indeed the overall comparison reveals the particular sensitivity of the drag to this wavelength as it suppresses most of the drag fluctuations, including the erratic ones, for both $Re = 800$ and $Re = 1000$. For the latter a further highlight is the recovery of the wake planar symmetry (figure 7) associated with the suppression of the helical mode.

3.1.3 Discussion

The above analysis clearly demonstrates the special receptivity of the flow, and of the resulting drag experienced by the bluff body, to the forcing at wavelength $\lambda_\theta = 2\pi/2$, and to a larger extent at wavelength $\lambda_\theta = 2\pi/3$. The receptivity of the flow to the forcing at $\lambda_\theta = 2\pi/2$ has to be set against the periodic observation of an azimuthal organization of the ternary lobes following a wavelength of $2\pi/2$. This pattern appears subsequently to the discharge of

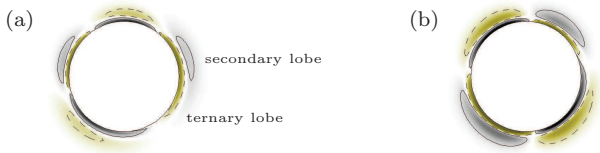

Fig. 8 Iso-contours and iso-lines of normalized streamwise vorticity (plain line: $\omega^+ = 0.01$, dashed line: $\omega^+ = -0.01$) at the base of the bluff body, for (a) $Re = 800$ and (b) $Re = 1000$.

the ternary lobes, associated with the vorticity bursts. It is illustrated in figure 8 in terms of contours of streamwise vorticity at the base of the bluff body for both $Re = 800$ and $Re = 1000$, as two pairs of counter-rotating ternary lobes (and two pairs of secondary lobes) distributed along the circumference of the trailing edge.

It is noticeable that a similar relationship between the receptivity of the flow to the forcing at wavelength $\lambda_\theta = 2\pi/1$ and the presence of an intrinsic instability of characteristic wavelength $2\pi/1$, that manifests through the transition of the unforced flow to the SS state [1,3,5], can be brought to the fore.

Conversely, despite the striking receptivity of the flow to the forcing at wavelength $\lambda_\theta = 2\pi/3$, the investigation of the unforced flow at both $Re = 800$ and $Re = 1000$ did not reveal the presence of a characteristic wake pattern associated with a wavelength of $2\pi/3$. However, if one considers that the efficiency of the distributed forcing at a given wavelength λ_θ is associated with the presence of an intrinsic instability characterized by the same wavelength λ_θ, then one can expect the $\lambda_\theta = 2\pi/3$ instability to be inherent to the flow, still latent, and prompt to emerge at higher Reynolds numbers. This hypothesis can be related to the conclusion of [9] on the distributed forcing of the flow past a 2D circular cylinder. In this work the authors have demonstrated that the flow response to a distributed forcing is optimal when the forcing wavelength matches the mode A characteristic wavelength, even for low Reynolds numbers where the flow has not yet undergone the transition to this three-dimensional mode.

3.2 Influence of the forcing amplitude and waveform

In this last section we briefly address the influence of the forcing amplitude and waveform on the drag coefficient. To this avail we focus on the distributed forcing at wavelength $\lambda_\theta = 2\pi/3$ for which the flow has shown to be the most receptive. The analysis relies on time histories of the drag coefficient. For sake of conciseness the contours of streamwise vorticity downstream of the bluff body are not shown as they do not highlight new flow features and are similar to that previously observed on figure 6 at $\lambda_\theta = 2\pi/3$.

In a first step the forcing amplitude α is varied from 0 (unforced flow) to 15% of the free stream velocity. Figure 10(a) shows that the large ampli-

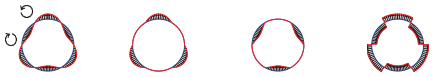

Fig. 9 Illustration of the sine, positive sine, negative sine and square waveforms at wavelength $\lambda_\theta = 2\pi/3$, from left to right. Circular arrows, given as an example for the sine waveform, indicate maxima of forcing-induced streamwise vorticity (direction of the arrows indicates its sign), at the inflection points of the forcing signal.

tude/low frequency drag oscillations associated with the vorticity bursts are progressively damped as the forcing amplitude is increased, up to their suppression at $\alpha = 7.5\%$. At this stage the drag oscillations associated with the vortex shedding are still visible, though strongly mitigated. The latter are eventually annihilated as α exceeds 10%. In parallel the mean drag coefficient increases with α. This might be attributed to a streamwise vorticity surplus promoted by larger azimuthal gradients of radial velocities in the forcing region (shown for illustrative purposes on figure 9).

Figure 10(b) shows the impact of the forcing waveform ξ on the drag history of the bluff body. Here ξ successively stands for a sine, positive sine (blowing is active, suction is turned off), negative sine (blowing is turned off, suction is active) and square function (see figure 9 for an illustration of the waveforms). For ξ defined as a positive sine, the forcing does not fundamentally alter the drag coefficient history. The drag oscillations, primarily induced by the vorticity bursts, display similar amplitudes to that of the unforced case, despite a slight increase of the normalized frequency St_b. Furthermore the mean drag coefficient $\bar{C_D}$ remains roughly unchanged. In contrast, for ξ defined as a negative sine, the impact of the forcing significantly alters the signature of vorticity bursts as large amplitude oscillations vanish, highlighting the residual small amplitude oscillations associated with the vortex shedding. In addition the mean drag coefficient is slightly reduced, down to $\bar{C_D} \approx 0.672$.

Finally, while 1) blowing alone has no significant effect on the drag history experienced by the bluff body and 2) suction alone both alters drag oscillations and mean value, intriguingly, combining both blowing and suction into a pure sine-type forcing completely suppresses the drag oscillations and increases the mean drag up to $\bar{C_D} \approx 0.684$. These observations once again suggest the nonlinear coupling effects between locally decelerated and accelerated regions associated with blowing and suction respectively. They also emphasize the role of forcing-induced streamwise vorticity, enhanced for the sine and square-type waveforms in comparison with the sole use of blowing or suction, on the stabilization of the ternary lobes.

4 Conclusion

In this work we have investigated the influence of a distributed forcing on the flow past a blunt-based axisymmetric bluff body of length-to-diameter ratio $L/D = 7$ at $Re = 800$ and $Re = 1000$. The forcing has been applied

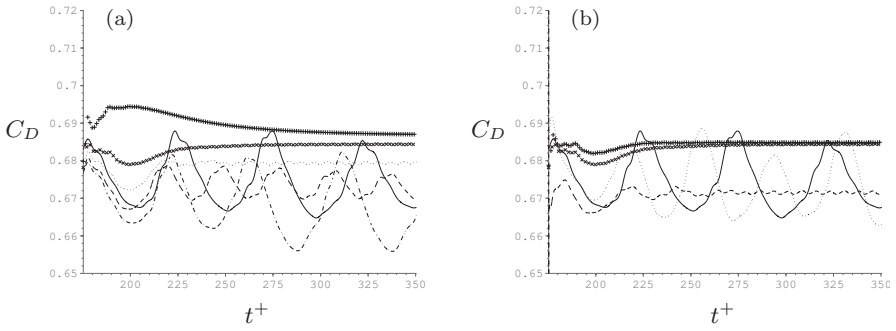

Fig. 10 Time history of the drag coefficient C_D as a function of (a) the forcing amplitude α and (b) the forcing waveform ξ, for $\lambda_\theta = 2\pi/3$ at $Re = 800$. ξ is a sine function in (a) and α is fixed to 10% in (b). In (a): — unforced; $\cdot-$ $\alpha = 2.5\%$; $--$ $\alpha = 5\%$; $\cdots$ $\alpha = 7.5\%$; $\times$ $\alpha = 10\%$; $+$ $\alpha = 15\%$. In (b): — unforced; $\cdots$ positive sine; $--$ negative sine; $\times$ sine; $+$ square.

via consecutive blowing and suction regions azimuthally distributed along the trailing edge of the bluff body. We have examined the impact of the forcing wavelength, amplitude and waveform on the drag experienced by the bluff body and on the occurrence of the reflectional symmetry preserving (RSP) and reflectional symmetry breaking (RSB) wake modes.

In a first step we bring to the fore the efficiency of the blowing/suction-type forcing at wavelength $\lambda_\theta = 2\pi/1$ in annihilating the large amplitude/low frequency drag oscillations induced by the periodic vorticity bursts, and at wavelength $\lambda_\theta = 2\pi/2$ in drastically damping both the large amplitude/low frequency drag oscillations and the low amplitude/high frequency oscillations induced by the vortex shedding. Furthermore the $\lambda_\theta = 2\pi/2$ forcing is shown to locally break down the reflectional symmetry typical of the unforced flow at $Re = 800$. In light of the fact that such wavelengths are identified as inherent to the unforced flow, the $\lambda_\theta = 2\pi/1$ and $\lambda_\theta = 2\pi/2$ forcing efficiency suggests the special receptivity of the flow to a forcing wavelength that matches intrinsic wavelength. Interestingly enough, it is revealed that forcing the flow at $\lambda_\theta = 2\pi/3$ has an even more dramatic effect on the drag history experienced by the bluff body since it also alleviates the erratic fluctuations typical of the chaotic regime above $Re = 790$. At $Re = 1000$ this effect is concomitant to the recovery of the planar symmetry of the wake, *i.e.* to the suppression of the helical mode. Following the previous argumentation, one can thus presuppose the $\lambda_\theta = 2\pi/3$ instability to be inherent to the flow, still latent, and prompt to emerge at higher Reynolds numbers. Finally the decrease of the forcing wavelength down to $\lambda_\theta = 2\pi/5$ tends to restore the main properties of the unforced flow.

In a second step the overall parameter analysis demonstrates that the blowing/suction-type forcing acts in lieu of fluidic vortex generators through the production of a streamwise vorticity surplus that tends to stabilize the ternary vorticity lobes observed at the aft part of the bluff body. Such forcing

further involves strong nonlinear interactions between locally decelerated and accelerated regions, severely affecting both the mean drag and the frequencies representative of the vortex shedding and vorticity bursts.

Acknowledgements The authors gratefully acknowledge the French Ministry of Defence and the DGA for supporting this work.

References

1. Bohorquez, P., Sanmiguel-Rojas, E., Sevilla, A., Jimenez-Gonzalez, J.I., Martinez-Bazan, C.: Stability and dynamics of the laminar wake past a slender blunt-based axisymmetric body. J. Fluid Mech. **676**, 110-144 (2011)
2. Bohorquez, P., Parras, L.: Three-dimensional numerical simulation of the wake flow of an afterbody at subsonic speeds. Theor. Comput. Fluid Dyn. DOI: 10.1007/s00162-011-0251-9 (2011)
3. Bury, Y., Jardin, T.: Transitions to chaos in the wake of an axisymmetric bluff body. Phys. Letters A DOI: 10.1016/j.physleta.2012.09.011 (2012)
4. Choi, H., Jeon, W.P., Kim, J.: Control of flow over a bluff body. Annu. Rev. Fluid Mech. **40**, 113-139 (2008)
5. Fabre, D., Auguste, F., Magnaudet, J.: Bifurcations and symmetry breaking in the wake of axisymmetric bodies. Phys. Fluids **20**, 051702 (2008)
6. Jardin, T., Bury, Y.: Spectral and lagrangian analysis of the forced flow past a circular cylinder using pulsed tangential jets. J. Fluid Mech. **696**, 285-300 (2012)
7. Jukes, T.N., Choi, K.S.: Control of unsteady flow separation over a circular cylinder using dielectric-barrier-discharge surface plasma. Phys. Fluids **21**, 094106 (2009)
8. Kim, J., Hahn, S., Kim, J., Lee, D.K., Choi, J., Jeon, W.P., Choi, H.: Active control of turbulent flow over a model vehicle for drag reduction. J. Turbul. **5**, 19 (2004)
9. Kim, J., Choi, H.: Distributed forcing of the flow over a circular cylinder. Phys. Fluids **17**, 033103 (2005)
10. Poncet, P., Hildebrand, R., Cottet, G.H., Koumoutsakos, P.: Spatially distributed control for optimal drag reduction of the flow past a circular cylinder. J. Fluid Mech. **599**, 111-120 (2008)
11. Seidel, J., Siegel, S., Cohen, K., McLaughlin, T.: Simulations of flow control of the wake behind an axisymmetric bluff body. In: 3^{rd} AIAA Flow Control Conference, art. no. 2006-3490 (2006)
12. Seidel, J., Siegel, S., Jeans, T., Aradag, S., Cohen, K., McLaughlin, T.: Analysis of an axisymmetric bluff body wake using Fourier transform and POD. In: 46^{th} AIAA Aerospace Sciences Meeting and Exhibit, art. no. 2008-0552 (2008)
13. Tomboulides, A.G., Orszag, S.A.: Numerical investigation of transitional and weak turbulent flow past a sphere. J. Fluid Mech. **416**, 51-73 (2000)